The Astronomical Journal, 166:226 (7pp), 2023 December https://doi.org/10.3847/1538-3881/acffc1

An Investigation of New Brown Dwarf Spectral Binary Candidates From the Backyard Worlds: Planet 9 Citizen Science Initiative

Alexia Bravo[1], Adam C. Schneider[1], Daniella Bardalez Gagliuffi[2], Adam J. Burgasser[3], Aaron M. Meisner[4], J. Davy Kirkpatrick[5], Jacqueline K. Faherty[6], Marc J. Kuchner[7], Dan Caselden[6], Arttu Sainio[8], and Les Hamlet[8]
The Backyard Worlds: Planet 9 Collaboration

[1] United States Naval Observatory, Flagstaff Station, 10391 West Naval Observatory Road, Flagstaff, AZ 86005, USA
[2] Department of Physics & Astronomy, Amherst College, 25 East Drive, Amherst, MA 01003, USA
[3] Department of Astronomy & Astrophysics, University of California San Diego, La Jolla, CA 92093, USA
[4] NSF's National Optical-Infrared Astronomy Research Laboratory, 950 N. Cherry Avenue, Tucson, AZ 85719, USA
[5] IPAC, Mail Code 100-22, Caltech, 1200 E. California Boulevard, Pasadena, CA 91125, USA
[6] Department of Astrophysics, American Museum of Natural History, Central Park West at 79th Street, New York, NY 10024, USA
[7] Exoplanets and Stellar Astrophysics Laboratory, NASA Goddard Space Flight Center, 8800 Greenbelt Road, Greenbelt, MD 20771, USA
[8] Backyard Worlds: Planet 9, USA
Received 2023 August 8; revised 2023 September 29; accepted 2023 October 2; published 2023 November 6

Abstract

We present three new brown dwarf spectral-binary candidates: CWISE J072708.09−360729.2, CWISE J103604.84−514424.4, and CWISE J134446.62−732053.9, discovered by citizen scientists through the Backyard Worlds: Planet 9 project. Follow-up near-infrared spectroscopy shows that each of these objects is poorly fit by a single near-infrared standard. We constructed binary templates and found significantly better fits, with component types of L7+T4 for CWISE J072708.09−360729.2, L7+T4 for CWISE J103604.84−514424.4, and L7+T7 for CWISE J134446.62−732053.9. However, further investigation of available spectroscopic indices for evidence of binarity and large amplitude variability suggests that CWISE J072708.09−360729.2 may instead be a strong variability candidate. Our analysis offers tentative evidence and characterization of these peculiar brown dwarf sources, emphasizing their value as promising targets for future high-resolution imaging or photometric variability studies.

Unified Astronomy Thesaurus concepts: Brown dwarfs (185); L dwarfs (894); T dwarfs (1679); Binary stars (154)

1. Introduction

Brown dwarfs occupy a unique space between stars and planets, possessing masses below the threshold required for sustained hydrogen fusion in their cores (Kumar 1962; Hayashi & Nakano 1963; Kumar 1963). Their cool temperatures and intrinsic faintness make them difficult to detect, and nearby brown dwarfs are continuing to be discovered (e.g., Marocco et al. 2019; Bardalez Gagliuffi et al. 2020; Best et al. 2020; Meisner et al. 2020a, 2020b; Kirkpatrick et al. 2021a, 2021b; Schneider et al. 2021; Kota et al. 2022; Lodieu et al. 2022; Schapera et al. 2022). The Backyard Worlds: Planet 9 project (Kuchner et al. 2017) leverages the collaboration between citizen and professional scientists to locate nearby substellar objects by identifying and analyzing moving objects in images from the Wide-field Infrared Survey Explorer (Wright et al. 2010; Mainzer et al. 2014). Multiepoch WISE images and motion measurements from WISE data (CatWISE 2020; Marocco et al. 2021) have allowed for numerous discoveries missed by previous surveys, many of which were based solely on infrared colors or limited to nearby objects with very large proper motions. In addition to finding new nearby brown dwarfs, the Backyard Worlds project has been adept at discovering unusual substellar objects, such as old, low-metallicity subdwarfs (Schneider et al. 2020; Meisner et al. 2021; Brooks et al. 2022) and comoving companions (Faherty et al. 2020, 2021; Jalowiczor et al. 2021; Kiwy et al. 2021, 2022; Rothermich et al. 2021; Gramaize et al. 2022; Softich et al. 2022). In this study, we examine three spectrally peculiar brown dwarfs found in the Backyard Worlds program: CWISE J072708.09−360729.2 (W0727−3607), CWISE J103604.84−514424.4 (W1036−5144), and CWISE J134446.62−732053.9 (W1344−7320). These objects were discovered by citizen scientists Dan Caselden, Arttu Sainio, and Les Hamlet. Each were flagged as high-priority for follow-up observations because their photometry and estimated spectral types indicated that they may be nearby ($d < 25$ pc). Properties of these three sources are provided in Table 1.

2. Observations

W0727−3607, W1036−5144, and W1344−7320 were observed with the TripleSpec4.1 near-infrared spectrograph (Schlawin et al. 2014; Herter et al. 2020) located at the Southern Astrophysical Research (SOAR) telescope. TripleSpec4.1 simultaneously covers 0.8−2.4 μm using six cross-dispersed orders with a resolving power of ∼3500. The observations were conducted in AEON queue mode and took place on 2023 April 16 (UT), 2023 February 10 (UT), and 2023 March 14 (UT) for W0727−3607, W1036−5144, and W1344−7320, respectively. The spectra were obtained in an ABBA pattern with 120 second exposures. The total integration times for W0727−3607, W1036−5144, and W1344−7320 were 2880, 2400, and 1920 s, respectively. A0 stars were observed immediately after each science target for telluric correction and flux calibration. Data reduction and telluric correction was performed using a modified version of the Spextool

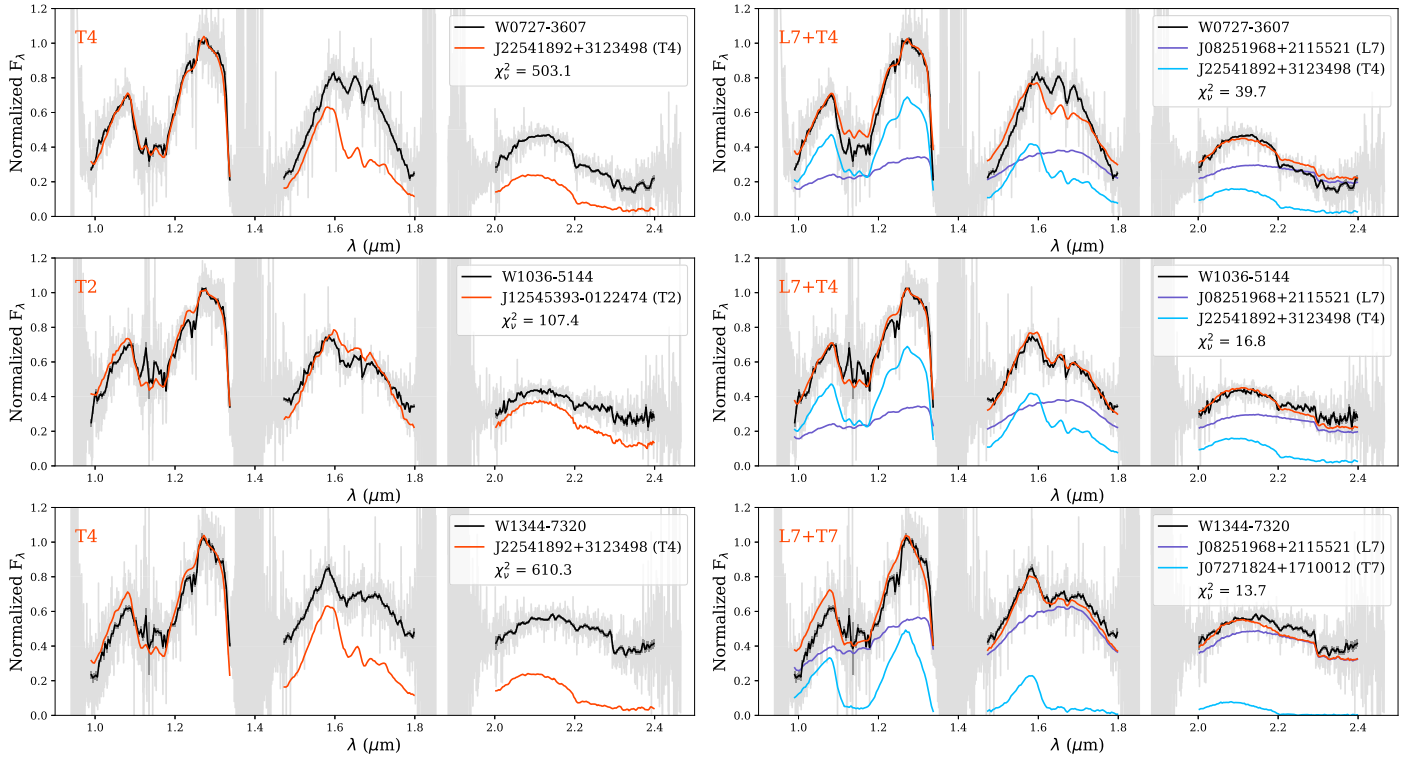

Figure 1. Observed SOAR/TripleSpec4.1 spectra for W0727−3607 (top), W1036−5144 (middle), and W1344−7320 (bottom), with gray lines showing the full resolution and black lines showing the spectra smoothed to the resolution of the standards and binary templates ($R \approx 150$) according to their parallax-based absolute fluxes. The left-hand column depicts the best-fitting single standards (orange line) for the spectra of the three candidates while the right-hand column shows both the binary template (orange line) and the standard spectra that compose it (purple line for primary, blue line for secondary). Reduced χ^2_ν values are reported for each of the fits.

Table 1
Candidate Spectral Binary Properties[a]

CatWISE Name	J (mag)	K_S (mag)	μ_α (mas yr^{-1})	μ_δ (mas yr^{-1})	SpT (single)	SpT (binary)
CWISE J072708.09−360729.2	16.521 ± 0.017	15.344 ± 0.026	−54.0 ± 8.3	233.6 ± 9.3	T4	L7+T4
CWISE J103604.84−514424.4	15.977 ± 0.012	14.776 ± 0.015	−108.1 ± 6.8	−62.7 ± 8.0	T2	L7+T4
CWISE J134446.62−732053.9	15.890 ± 0.087	14.185 ± 0.010	−34.3 ± 5.4	143.3 ± 6.7	T4	L7+T7

Note.
[a] All near-infrared photometry comes from the Vista Hemisphere Survey (VHS; McMahon et al. 2013), with the exception of the J-band magnitude of CWISE J134446.62−732053.9, which comes from 2MASS (Skrutskie et al. 2006). All proper motions listed are taken from the CatWISE 2020 catalog (Marocco et al. 2021).

data reduction package (Vacca et al. 2003; Cushing et al. 2004). The final reduced spectra are shown in Figure 1.

3. Analysis

To determine preliminary spectral types, we compared to the near-infrared L and T dwarf standards from Kirkpatrick et al. (2010) and Burgasser et al. (2006b), with the exception of the L7 standard, where we use 2MASSI J0825196 + 211552 as recommended in Cruz et al. (2018), as the original L7 near-infrared standard appears to have an unusually low surface gravity and age. The best-fitting standards for each object are shown in the left column of Figure 1, and match reasonably well in the J-band region, but show significant discrepancies beyond ∼1.5 μm. To ensure that differences between standards and the observed spectra were not due to uncertainties incurred when stitching orders or some other observational systematic, we calculated synthetic photometric $J - K_S$ colors using the VISTA filter response curves. We find synthetic colors consistent with the photometric colors in Table 1 to within 1σ. For this reason, we constructed binary templates in an attempt to better fit the observed spectra.

We utilized the same spectral standards as above, with a few exceptions to account for known distance and multiplicity. The L2 near-infrared standard is a resolved binary (Liu & Leggett 2005), so we instead use the L2 object 2MASS J04082905−1450334 (Wilson et al. 2003; Bardalez Gagliuffi et al. 2014). The L5 near-infrared standard 2MASS J08350622+1953050 has no measured parallax, so we instead use the L5 2MASS J21373742+0808463 (Reid et al. 2008; Burgasser et al. 2010). The T0 near-infrared standard is suspected to be a spectral binary (Burgasser et al. 2010; Ashraf et al. 2022), thus we employed the T0 WISEPA J015010.86+382724.3 (Kirkpatrick et al. 2011). Lastly, the T3 standard 2MASS J12095613−1004008 is a resolved binary (Liu et al. 2010), and we therefore use the T3 WISEPC J223937.55 +161716.2 (Kirkpatrick et al. 2011). The objects used to create spectral binary templates are summarized in Table 2.

Table 2
Properties of Objects Used to Create Binary Templates

SpT	Discovery Name	Discovery Reference	Spec. Reference	J (mag)	Reference	ϖ (mas)	Reference
L0	2MASSP J0345432+254023	1	15	13.924 ± 0.003	23	37.89 ± 0.26	27
L1	2MASS J21304464−0845205	2	16	14.059 ± 0.002	24	37.47 ± 0.31	27
L2	2MASS J04082905−1450334[a]	3	16	14.128 ± 0.002	24	45.57 ± 0.27	27
L3	2MASSW J1506544+132106	4	17	13.211 ± 0.002	25	85.43 ± 0.19	27
L4	2MASS J21580457−1550098	2	16	14.794 ± 0.004	24	43.11 ± 0.91	27
L5	2MASS J21373742+0808463[b]	5	18	14.644 ± 0.005	25	66.37 ± 0.66	27
L6	2MASSI J1010148−040649	6	19	15.372 ± 0.005	24	57.7 ± 3.6	28
L7	2MASSI J0825196+211552	7	18	15.014 ± 0.005	25	93.19 ± 0.59	29
L8	2MASSW J1632291+190441	8	17	15.823 ± 0.010	25	66.29 ± 1.61	29
L9	DENIS J025503.3−470049	9	20	13.122 ± 0.001	24	205.43 ± 0.19	27
T0	WISEPA J015010.86+382724.3[c]	10	10	15.901 ± 0.010	25	44.6 ± 3.2	28
T1	SDSS J083717.21−000018.0	11	20	16.929 ± 0.007	26	29.8 ± 2.7	30
T2	SDSS J125453.90−012247.5	11	21	14.694 ± 0.002	26	78.34 ± 1.07	29
T3	WISEPC J223937.55+161716.2[d]	10	10	15.995 ± 0.010	25	42.9 ± 3.0	30
T4	2MASSI J2254188+312349	12	21	15.000 ± 0.005	25	72.0 ± 3.0	31
T5	2MASS J15031961+2525196	13	21	13.621 ± 0.003	25	155.78 ± 0.76	27
T6	SDSSp J162414.37+002915.6	14	22	15.187 ± 0.006	25	90.9 ± 1.2	32
T7	2MASSI J0727182+171001	12	22	15.210 ± 0.006	25	112.5 ± 0.9	33
T8	2MASSI J0415195−093506	12	21	15.327 ± 0.004	24	175.2 ± 1.7	33

Notes.
[a] This object replaces the L2 near-infrared standard (Kelu-1), which is a resolved binary (Liu & Leggett 2005).
[b] This object replaces the L5 near-infrared standard (2MASS J08350622+1953050), which has no measured parallax.
[c] This object replaces the T0 near-infrared standard (2MASS J12074717+0244249), which is a suspected spectral binary (Burgasser et al. 2010).
[d] This object replaces the T3 near-infrared standard (2MASS J12095613−1004008), which is a resolved binary (Liu et al. 2010).
References. (1) Kirkpatrick et al. (1997); (2) Kirkpatrick et al. (2008); (3) Wilson et al. (2003); (4) Gizis et al. (2000); (5) Reid et al. (2008); (6) Cruz et al. (2003); (7) Kirkpatrick et al. (2000); (8) Kirkpatrick et al. (1999); (9) Martín et al. (1999); (10) Kirkpatrick et al. (2011); (11) Leggett et al. (2000); (12) Burgasser et al. (2002); (13) Burgasser et al. (2003); (14) Strauss et al. (1999); (15) Burgasser & McElwain (2006); (16) Bardalez Gagliuffi et al. (2014); (17) Burgasser (2007); (18) Burgasser et al. (2010); (19) Reid et al. (2006); (20) Burgasser et al. (2006b); (21) Burgasser et al. (2004); (22) Burgasser et al. (2006a); (23) Lawrence et al. (2007); (24) McMahon et al. (2013); (25) Dye et al. (2018); (26) Edge et al. (2013); (27) Gaia Collaboration et al. (2023); (28) Kirkpatrick et al. (2021a); (29) Dahn et al. (2017); (30) Best et al. (2020); (31) Manjavacas et al. (2013); (32) Tinney et al. (2003); (33) Dupuy & Liu (2012).

To generate spectral binary templates, we acquired near-infrared spectra from the the SpeX Prism Library Analysis Toolkit (SPLAT; Burgasser & Splat Development Team 2017). We absolute flux calibrated each spectrum using UKIDSS Hemisphere Survey (Dye et al. 2018) or Vista Hemisphere Survey (VHS; McMahon et al. 2013) J-band photometry, and measured parallaxes (Tinney et al. 2003; Dupuy & Liu 2012; Manjavacas et al. 2013; Dahn et al. 2017; Best et al. 2020; Kirkpatrick et al. 2021a; Gaia Collaboration et al. 2023). Finally, we added the spectra together and normalized the result to the J-band peak between 1.27 and 1.29 μm. We compared the resulting templates to each observed spectrum and found the best fits by calculating χ^2_ν values following Burgasser et al. (2010).

3.1. Spectral Index Calculations

Spectral indices are also used to identify potential objects of interest (e.g., young brown dwarfs, spectral binaries, and photometric variables). We follow the methods and calculate the indices defined in Burgasser et al. (2002, 2006b, 2010) and Bardalez Gagliuffi et al. (2014) for our observed objects (Table 3) and a large comparison sample from the SPLAT library. Uncertainties were determined in a Monte Carlo fashion. We use binary index regions from Burgasser et al. (2010)' and variability regions from Ashraf et al. (2022) in the following sections.

4. Results and Discussion

The observed discrepancies between observed spectra and existing spectral standards can be attributed to various factors —such as binarity, variability, youth, and metallicity—or a combination of these influences, as discussed below.

4.1. Binarity

4.1.1. Analysis of Binary Templates

The right column of Figure 1 compares the best-fitting binary templates to our sources. The discrepancies observed with the single fits beyond approximately 1.5 μm are greatly reduced with the binary templates, as verified by lower χ^2_ν values. A discussion of the results for each individual object follows.

CWISE J072708.09−360729.2: the best-fitting T4 single standard exhibits a significantly higher $\chi^2_\nu = 503$ compared to the L7+T4 binary template, which has $\chi^2_\nu = 39.7$. Following Burgasser et al. (2010), we evaluate our fits with a one-sided F-test, finding $\eta_{SB} = 12.7$, well above the $\eta_{SB} > 1.34$ spectral binary confidence threshold given in that work. Although the binary template provides a superior fit overall, discrepancies persist, particularly at the H-band peak. We retain W0727 −3607 as a spectral binary candidate, but discuss below that it is also a potential variable source (see Section 5).

CWISE J103604.84−514424.4: W1036−5144 shows a lower-than-expected peak in the H band and more flux across the K band compared to the T2 standard. These discrepancies

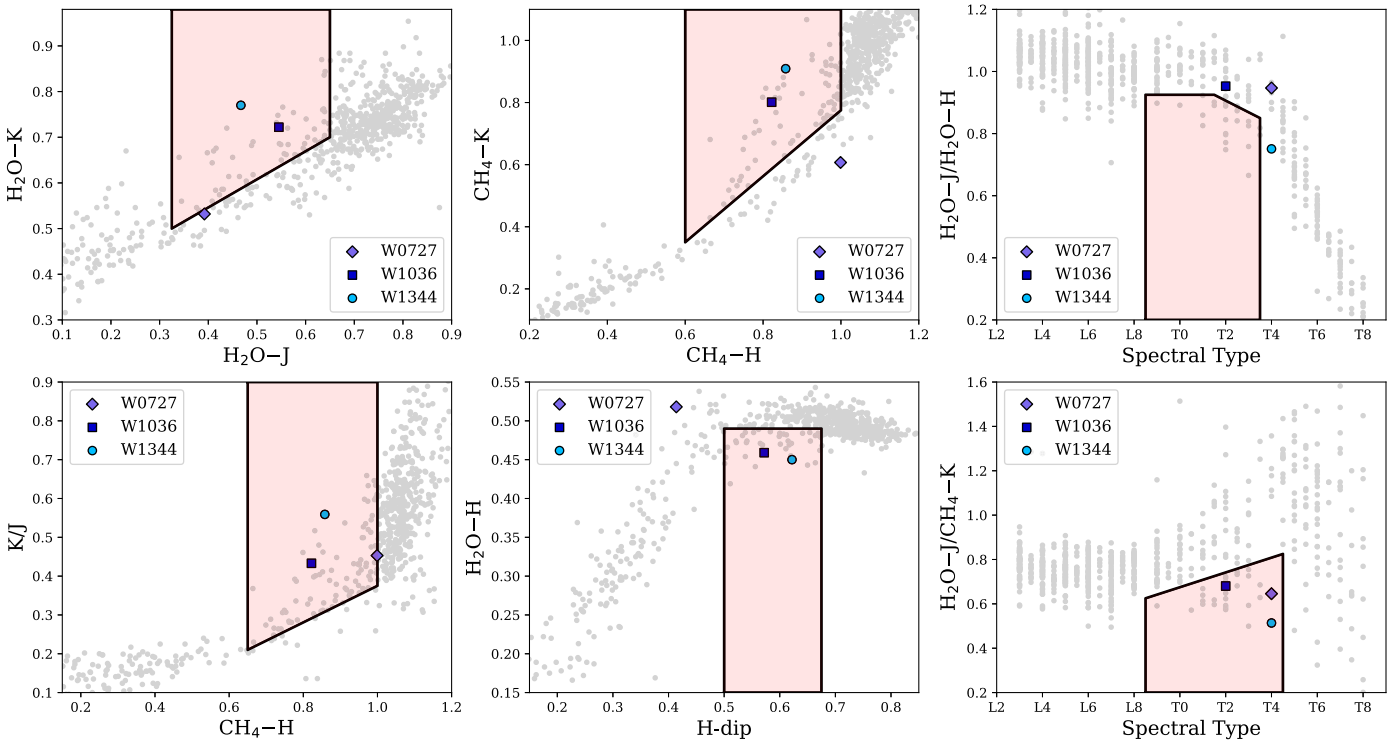

Figure 2. Index-index plots highlighting regions defined in Burgasser et al. (2010) and Bardalez Gagliuffi et al. (2015), as indicative of spectral binarity (red-shaded regions). Background gray points are SPLAT objects with spectral types between L3 and T8. The three targets of this study are shown in the legend.

Table 3
Spectral Index Values

Spectral Index	Object			Reference[a]
	W0727−3607	W1036−5144	W1344−7320	
H_2O-*J*	0.392 ± 0.009	0.546 ± 0.009	0.467 ± 0.017	1
CH_4-*J*	0.542 ± 0.006	0.586 ± 0.004	0.579 ± 0.010	1
J-Curve	4.121 ± 0.084	2.970 ± 0.042	3.286 ± 0.104	2
CH_4-*H*	0.999 ± 0.011	0.822 ± 0.005	0.858 ± 0.011	1
H-Bump	0.852 ± 0.012	1.120 ± 0.008	1.056 ± 0.016	2
H-Dip	0.518 ± 0.006	0.459 ± 0.003	0.451 ± 0.006	3
CH_4-*K*	0.607 ± 0.010	0.801 ± 0.009	0.909 ± 0.013	1
K-Slope	0.960 ± 0.010	0.975 ± 0.008	0.973 ± 0.012	4
K/*J*	0.453 ± 0.005	0.433 ± 0.003	0.559 ± 0.007	1
H_2O-*H*	0.414 ± 0.010	0.572 ± 0.006	0.622 ± 0.013	1
Binarity[b]	weak	strong	strong	
Variability[c]	strong	…	…	

Notes.
[a] Given reference corresponds to the work where the index was originally defined.
[b] Based on the index criteria defined in Burgasser et al. (2010).
[c] Based on the index criteria defined in Ashraf et al. (2022).
References. (1) Burgasser et al. (2006b); (2) Bardalez Gagliuffi et al. (2014); (3) Burgasser et al. (2010) Burgasser et al. (2002).

are largely resolved in the L7+T4 binary fit, with only minor deviations in the *J* band and in the longest wavelengths of the *K* band. The binary fit yields a significantly lower $\chi^2_\nu = 16.8$, compared to the $\chi^2_\nu = 107.4$ for the single fit, and yields $\eta_{SB} = 6.4$, consistent with the spectral binary criteria specified in Burgasser et al. (2010).

CWISE J134446.62−732053.9: the single standard fit to W1344−7320 has *H* and *K* bands that are underluminous, leading to a relatively poor $\chi^2_\nu = 610$. The L7+T7 binary template yields a significantly improved fit with $\chi^2_\nu = 13.7$. Although there is a slight discrepancy in *Y* band, where the template is too bright compared to the observed spectrum, the remainder of the *J*-, *H*-, and *K*-band regions exhibit a well-matched morphology. Our χ^2_ν values correspond to $\eta_{SB} = 44.5$, which again satisfies the spectral binary criteria specified in Burgasser et al. (2010).

4.1.2. Analysis of Binary Indices

The spectral indices shown to be indicative of binarity in Burgasser et al. (2010) are shown in Figure 2. That study designated sources that satisfied at least three index criteria as

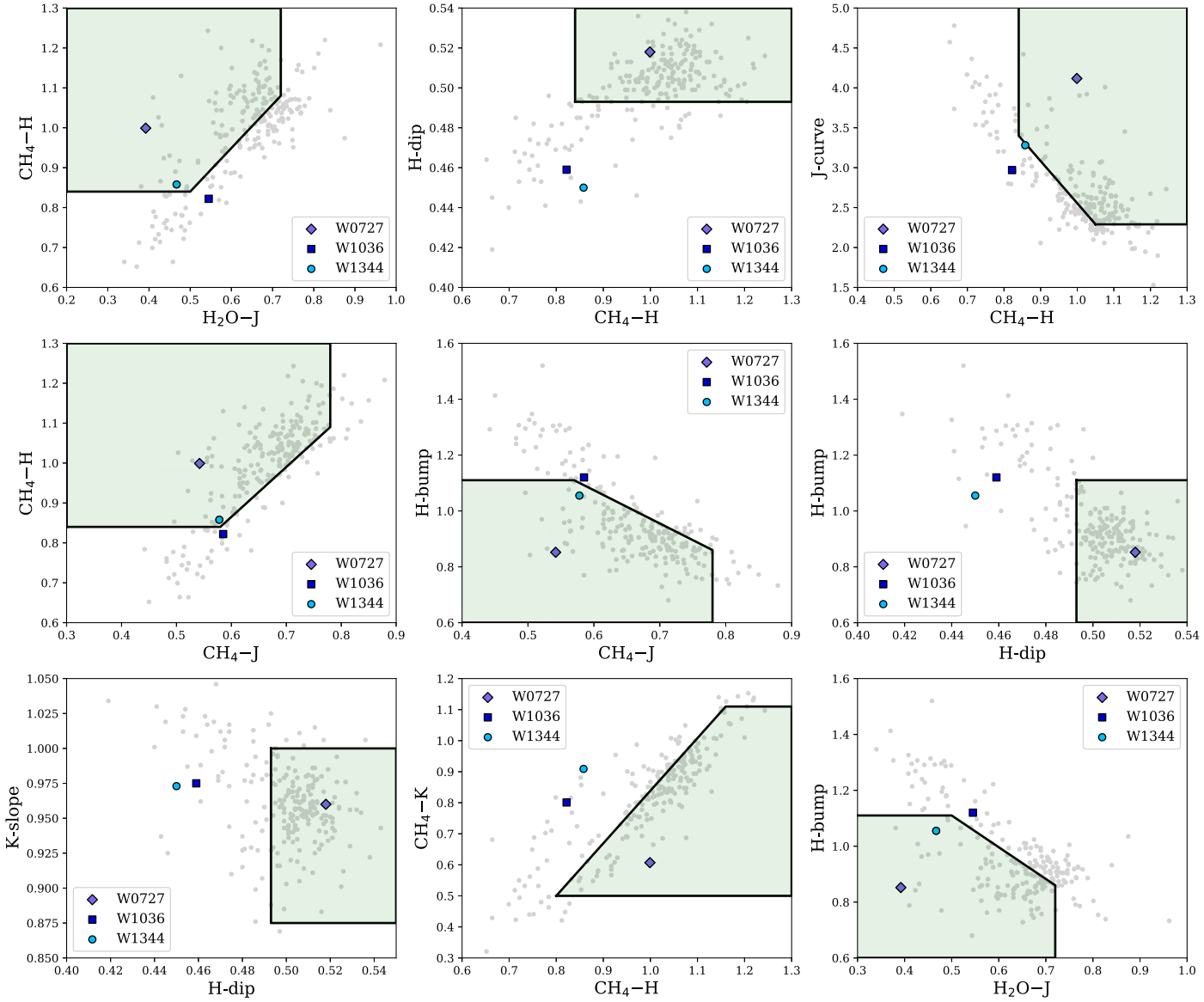

Figure 3. Index-index plots highlighting the regions indicative of photometric variability defined in Ashraf et al. (2022; green-shaded regions). Background gray points are SPLAT objects with spectral types between L7 and T3, with our three observed targets indicated shown in the legend.

"strong" candidates, and two index criteria as "weak" candidates.

CWISE J072708.09−360729.2: W0727−3607 falls within two of five regions indicative of binarity, and are very close to the edges of these regions. This classifies the source as a weak candidate. Note that we exclude for consideration the H_2O-J/H_2O-H versus spectral type comparison as it is not applicable for spectral types later than T3.5. Along with the mediocre fit of the L7+T4 binary template, this result suggests a factor other than binarity is responsible for this object's unusual spectrum.

CWISE J103604.84−514424.4: W1036−5144 satisfies five of six regions, making it a strong binary candidate. Considering the well-fit binary template, binarity is a strong possibility for this source.

CWISE J134446.62−732053.9: W1344−7320 satisfies five of five binary regions (excluding H_2O-J/H_2O-H versus spectral type), making it a strong binary candidate. Again, the well-fit binary template of L7+T7 makes this object a likely spectral binary.

4.1.3. Distance Estimation

If these objects are indeed spectral binaries, then updated distance estimates can be obtained by scaling the best-fitting absolutely flux calibrated binary templates to each object's observed photometric magnitudes. Using *J*-band photometry from VHS for W0727−3607 and W1036−5144 and 2MASS (Skrutskie et al. 2006) for W1344−7320, we find estimated distances of 34 ± 7 pc, 27 ± 5 pc, and 20 ± 4 pc, respectively.

4.2. Variability

There is evidence that some spectral binary candidates are instead single stars with inhomogeneous atmospheres as indicated via their photometric or spectroscopic variability (e.g., 2MASS J21392676+0220226; Radigan et al. 2012;

Khandrika et al. 2013). We applied the spectral index criteria introduced in Ashraf et al. (2022) to analyze the spectra of W0727−3607, W1036−5144, and W1344−7320 and evaluate their potential as strong variable sources. This method uses single low-resolution spectra to empirically identify spectral indices that may be indicative of variability based on known variable sources. The idea is that cloudy or patchy layers at different temperatures in a brown dwarf atmosphere that lead to photometric variability may have measurable effects in the emergent spectra of these objects. Note that we do not examine any index-index criteria that use the H_2O-K index, as the region of the numerator range (1.975−1.995 μm) is especially noisy in our TripleSpec4.1 spectra. In Figure 3, there are nine total index-index correlation plots, as discussed below. Ashraf et al. (2022) only considered objects that satisfied all of their variability index criteria as "strong" candidates, and those that satisfied all but one of their outlined criteria as "weak" candidates.

4.2.1. Analysis of Variable Indices

CWISE J072708.09−360729.2: W0727−3607 falls within all of the designated regions indicating potential variability. Coupled with the weak spectral binary designation and less accurate match to binary templates, variability appear to be at least partly responsible for the unusual shape of this object's spectrum. We investigated potential variability using WISE single-exposure photometry following the methods in Schneider et al. (2023). We found no clear signs of variability in the single-exposure WISE data, with W1 and W2 photometric standard deviation values within 1σ of the median value for objects with similar magnitudes. However, we note that with magnitudes of $W1 = 14.639 \pm 0.018$ mag and $W2 = 13.862 \pm 0.15$ mag, W0727−3607 may be too faint to detect significant variability in WISE data, as no variables were identified in Schneider et al. (2023) with magnitudes as faint as these.

CWISE J103604.84−514424.4: W1036−5144 consistently lies outside the range indicative of potential variability, supporting the spectral binary hypothesis.

CWISE J134446.62−732053.9: W1344−7320 satisfies four of the nine variability regions, below the weak candidate threshold of Ashraf et al. (2022) again, the spectral binary hypothesis is favored for this object.

5. Conclusions

In this study, we presented three new brown dwarf spectral binary candidates: CWISE J072708.09−360729.2, CWISE J103604.84−514424.4, and CWISE J134446.62−732053.9. By constructing binary templates and comparing them to the observed spectra, we found significantly better fits, revealing component types of T0+T7 for CWISE J072708.09−360729.2, L7+T4 for CWISE J103604.84−514424.4, and L7+T7 for CWISE J134446.62−732053.9. However, our investigation of variability indices suggests that CWISE J072708.09−360729.2 is a strong variability candidate.

The rarity of brown dwarf–brown dwarf binary systems, as consistently highlighted by statistical studies (Burgasser 2007; Radigan et al. 2013; Aberasturi et al. 2014; Opitz et al. 2016; Fontanive et al. 2018), underscores the importance of pinpointing more such systems. Moreover, the ability to identify spectral binaries offers the advantage that their orbital period are sufficiently short to be amenable to dynamical-mass follow up (Burgasser et al. 2012; Bardalez Gagliuffi et al. 2015; Burgasser et al. 2016; Sahlmann et al. 2020). Similarly, variable brown dwarfs provide opportunities to study their rotational and atmospheric dynamics, particularly through multiwavelength studies (Buenzli et al. 2012; Apai et al. 2013; Radigan et al. 2013). Future work includes confirming the binary and/or variability nature of these objects through high-resolution imaging and photometry, astrometric, and radial velocity monitoring. Increasing the sample of close binary and variable brown dwarfs has the potential to advance our understanding of substellar formation, evolution, and dynamics.

Acknowledgments

The authors acknowledge support from the Science and Engineering Appreticeship Program (SEAP) of the Office of Naval Research. The Backyard Worlds:Planet 9 team would like to thank the many Zooniverse volunteers who have participated in this project. We would also like to thank the Zooniverse web development team for their work creating and maintaining the Zooniverse platform and the Project Builder tools. This work is based on observations obtained at the Southern Astrophysical Research (SOAR) telescope, which is a joint project of the Ministério da Ciência, Tecnologia e Inovações (MCTI/LNA) do Brasil, the US National Science Foundation's NOIRLab, the University of North Carolina at Chapel Hill (UNC), and Michigan State University (MSU). This material is based upon work supported by the National Science Foundation under grant No. 2007068, 2009136, and 2009177. This publication makes use of data products from the Wide-field Infrared Survey Explorer, which is a joint project of the University of California, Los Angeles, and the Jet Propulsion Laboratory/California Institute of Technology, funded by the National Aeronautics and Space Administration. This publication also makes use of data products from NEOWISE, which is a project of the Jet Propulsion Laboratory/California Institute of Technology, funded by the Planetary Science Division of the National Aeronautics and Space Administration.

Facilities: SOAR, WISE.

Software: SPLAT (Burgasser & Splat Development Team 2017), Spextool (Vacca et al. 2003; Cushing et al. 2004).

ORCID iDs

Alexia Bravo https://orcid.org/0009-0002-3936-8059
Adam C. Schneider https://orcid.org/0000-0002-6294-5937
Daniella Bardalez Gagliuffi https://orcid.org/0000-0001-8170-7072
Adam J. Burgasser https://orcid.org/0000-0002-6523-9536
Aaron M. Meisner https://orcid.org/0000-0002-1125-7384
J. Davy Kirkpatrick https://orcid.org/0000-0003-4269-260X
Jacqueline K. Faherty https://orcid.org/0000-0001-6251-0573
Marc J. Kuchner https://orcid.org/0000-0002-2387-5489
Dan Caselden https://orcid.org/0000-0001-7896-5791
Arttu Sainio https://orcid.org/0000-0003-4864-5484
Les Hamlet https://orcid.org/0000-0002-7389-2092

References

Aberasturi, M., Burgasser, A. J., Mora, A., et al. 2014, AJ, 148, 129
Apai, D., Radigan, J., Buenzli, E., et al. 2013, ApJ, 768, 121

Ashraf, A., Bardalez Gagliuffi, D. C., Manjavacas, E., et al. 2022, ApJ, 934, 178
Bardalez Gagliuffi, D. C., Burgasser, A. J., Gelino, C. R., et al. 2014, ApJ, 794, 143
Bardalez Gagliuffi, D. C., Faherty, J. K., Schneider, A. C., et al. 2020, ApJ, 895, 145
Bardalez Gagliuffi, D. C., Gelino, C. R., & Burgasser, A. J. 2015, AJ, 150, 163
Best, W. M. J., Liu, M. C., Magnier, E. A., & Dupuy, T. J. 2020, AJ, 159, 257
Brooks, H., Kirkpatrick, J. D., Caselden, D., et al. 2022, AJ, 163, 47
Buenzli, E., Apai, D., Morley, C. V., et al. 2012, ApJL, 760, L31
Burgasser, A. J. 2007, ApJ, 659, 655
Burgasser, A. J. & Splat Development Team 2017, in ASI Conf. Ser. 14, ed. P. Coelho, L. Martins, & E. Griffin (Hyderabad: Astronomical Society of India), 7
Burgasser, A. J., Blake, C. H., Gelino, C. R., Sahlmann, J., & Bardalez Gagliuffi, D. 2016, ApJ, 827, 25
Burgasser, A. J., Burrows, A., & Kirkpatrick, J. D. 2006a, ApJ, 639, 1095
Burgasser, A. J., Cruz, K. L., Cushing, M., et al. 2010, ApJ, 710, 1142
Burgasser, A. J., Geballe, T. R., Leggett, S. K., Kirkpatrick, J. D., & Golimowski, D. A. 2006b, ApJ, 637, 1067
Burgasser, A. J., Kirkpatrick, J. D., Brown, M. E., et al. 2002, ApJ, 564, 421
Burgasser, A. J., Kirkpatrick, J. D., McElwain, M. W., et al. 2003, AJ, 125, 850
Burgasser, A. J., Luk, C., Dhital, S., et al. 2012, ApJ, 757, 110
Burgasser, A. J., & McElwain, M. W. 2006, AJ, 131, 1007
Burgasser, A. J., McElwain, M. W., Kirkpatrick, J. D., et al. 2004, AJ, 127, 2856
Cruz, K. L., Núñez, A., Burgasser, A. J., et al. 2018, AJ, 155, 34
Cruz, K. L., Reid, I. N., Liebert, J., Kirkpatrick, J. D., & Lowrance, P. J. 2003, AJ, 126, 2421
Cushing, M. C., Vacca, W. D., & Rayner, J. T. 2004, PASP, 116, 362
Dahn, C. C., Harris, H. C., Subasavage, J. P., et al. 2017, AJ, 154, 147
Dupuy, T. J., & Liu, M. C. 2012, ApJS, 201, 19
Dye, S., Lawrence, A., Read, M. A., et al. 2018, MNRAS, 473, 5113
Edge, A., Sutherland, W., Kuijken, K., et al. 2013, Msngr, 154, 32
Faherty, J. K., Gagné, J., Popinchalk, M., et al. 2021, ApJ, 923, 48
Faherty, J. K., Goodman, S., Caselden, D., et al. 2020, ApJ, 889, 176
Fontanive, C., Biller, B., Bonavita, M., & Allers, K. 2018, MNRAS, 479, 2702
Gaia Collaboration, Vallenari, A., Brown, A. G. A., et al. 2023, A&A, 674, A1
Gizis, J. E., Monet, D. G., Reid, I. N., et al. 2000, AJ, 120, 1085
Gramaize, L., Schneider, A. C., Marocco, F., et al. 2022, RNAAS, 6, 229
Hayashi, C., & Nakano, T. 1963, PThPh, 30, 460
Herter, T., Henderson, C., Bonati, M., et al. 2020, Proc. SPIE, 11447, 114476L
Jalowiczor, P. A., Casewell, S., Schneider, A. C., et al. 2021, RNAAS, 5, 76
Khandrika, H., Burgasser, A. J., Melis, C., et al. 2013, AJ, 145, 71
Kirkpatrick, J. D., Beichman, C. A., & Skrutskie, M. F. 1997, ApJ, 476, 311
Kirkpatrick, J. D., Cruz, K. L., Barman, T. S., et al. 2008, ApJ, 689, 1295
Kirkpatrick, J. D., Cushing, M. C., Gelino, C. R., et al. 2011, ApJS, 197, 19
Kirkpatrick, J. D., Gelino, C. R., Faherty, J. K., et al. 2021a, ApJS, 253, 7
Kirkpatrick, J. D., Looper, D. L., Burgasser, A. J., et al. 2010, ApJS, 190, 100
Kirkpatrick, J. D., Marocco, F., Caselden, D., et al. 2021b, ApJL, 915, L6
Kirkpatrick, J. D., Reid, I. N., Liebert, J., et al. 1999, ApJ, 519, 802
Kirkpatrick, J. D., Reid, I. N., Liebert, J., et al. 2000, AJ, 120, 447
Kiwy, F., Faherty, J., Meisner, A., et al. 2021, RNAAS, 5, 196
Kiwy, F., Faherty, J. K., Meisner, A., et al. 2022, AJ, 164, 3
Kota, T., Kirkpatrick, J. D., Caselden, D., et al. 2022, AJ, 163, 116
Kuchner, M. J., Faherty, J. K., Schneider, A. C., et al. 2017, ApJL, 841, L19
Kumar, S. S. 1962, AJ, 67, 579
Kumar, S. S. 1963, ApJ, 137, 1121
Lawrence, A., Warren, S. J., Almaini, O., et al. 2007, MNRAS, 379, 1599
Leggett, S. K., Geballe, T. R., Fan, X., et al. 2000, ApJL, 536, L35
Liu, M. C., Dupuy, T. J., & Leggett, S. K. 2010, ApJ, 722, 311
Liu, M. C., & Leggett, S. K. 2005, ApJ, 634, 616
Lodieu, N., Zapatero Osorio, M. R., Martín, E. L., Rebolo López, R., & Gauza, B. 2022, A&A, 663, A84
Mainzer, A., Bauer, J., Cutri, R. M., et al. 2014, ApJ, 792, 30
Manjavacas, E., Goldman, B., Reffert, S., & Henning, T. 2013, A&A, 560, A52
Marocco, F., Caselden, D., Meisner, A. M., et al. 2019, ApJ, 881, 17
Marocco, F., Eisenhardt, P. R. M., Fowler, J. W., et al. 2021, ApJS, 253, 8
Martín, E. L., Delfosse, X., Basri, G., et al. 1999, AJ, 118, 2466
McMahon, R. G., Banerji, M., Gonzalez, E., et al. 2013, Msngr, 154, 35
Meisner, A. M., Caselden, D., Kirkpatrick, J. D., et al. 2020a, ApJ, 889, 74
Meisner, A. M., Faherty, J. K., Kirkpatrick, J. D., et al. 2020b, ApJ, 899, 123
Meisner, A. M., Schneider, A. C., Burgasser, A. J., et al. 2021, ApJ, 915, 120
Opitz, D., Tinney, C. G., Faherty, J. K., et al. 2016, ApJ, 819, 17
Radigan, J., Jayawardhana, R., Lafrenière, D., et al. 2012, ApJ, 750, 105
Radigan, J., Jayawardhana, R., Lafrenière, D., et al. 2013, ApJ, 778, 36
Reid, I. N., Cruz, K. L., Kirkpatrick, J. D., et al. 2008, AJ, 136, 1290
Reid, I. N., Lewitus, E., Allen, P. R., Cruz, K. L., & Burgasser, A. J. 2006, AJ, 132, 891
Rothermich, A., Schneider, A. C., Faherty, J. K., et al. 2021, RNAAS, 5, 18
Sahlmann, J., Burgasser, A. J., Bardalez Gagliuffi, D. C., et al. 2020, MNRAS, 495, 1136
Schapera, N., Caselden, D., Meisner, A. M., et al. 2022, RNAAS, 6, 189
Schlawin, E., Herter, T. L., Henderson, C., et al. 2014, Proc. SPIE, 9147, 91472H
Schneider, A. C., Burgasser, A. J., Bruursema, J., et al. 2023, ApJL, 943, L16
Schneider, A. C., Burgasser, A. J., Gerasimov, R., et al. 2020, ApJ, 898, 77
Schneider, A. C., Meisner, A. M., Gagné, J., et al. 2021, ApJ, 921, 140
Skrutskie, M. F., Cutri, R. M., Stiening, R., et al. 2006, AJ, 131, 1163
Softich, E., Schneider, A. C., Patience, J., et al. 2022, ApJL, 926, L12
Strauss, M. A., Fan, X., Gunn, J. E., et al. 1999, ApJL, 522, L61
Tinney, C. G., Burgasser, A. J., & Kirkpatrick, J. D. 2003, AJ, 126, 975
Vacca, W. D., Cushing, M. C., & Rayner, J. T. 2003, PASP, 115, 389
Wilson, J. C., Miller, N. A., Gizis, J. E., et al. 2003, in IAU Symp. 211, Brown Dwarfs, ed. E. Martín (San Francisco, CA: ASP), 197
Wright, E. L., Eisenhardt, P. R. M., Mainzer, A. K., et al. 2010, AJ, 140, 1868